Resonant indirect processes in electron-impact single ionization of Ne^{7+} ions

K. Aichele, W. Shi, F. Scheuermann, H. Teng, E. Salzborn, and A. Müller
Institut für Kernphysik, Universität Giessen, D-35392 Giessen, Germany
(Received 6 June 2000; published 6 December 2000)

We present a detailed experimental and theoretical study of electron-impact single ionization of Ne^{7+}. High-resolution and high-precision energy-scan measurements of the *K*-shell excitation threshold region have been performed with statistical uncertainties as low as 0.036% and an energy stepwidth of 0.39 eV. Resonance features in the cross section of Ne^{7+} arising from indirect ionization processes have been observed. A new unified *R*-matrix calculation of the ionization cross section very well reproduces most of the features observed in the experiment.

DOI: 10.1103/PhysRevA.63.014701 PACS number(s): 34.80.Dp, 34.80.Kw

Resonant indirect ionization processes in electron-impact ionization of ions have been a subject of great interest since the first theoretical introduction of the concept [1,2]. Significant progress in the study of resonant ionization processes has been made both experimentally and theoretically, subsequent to the first unambiguous experimental observation of the basic mechanisms [3,4]. On the theoretical side, most calculations employed the independent-process approximation (see the review by Moores and Reed [5]). Recently a new *R*-matrix approach was introduced by Berrington *et al.* [6], which treated direct and indirect ionization processes in a unified way. Hence the possibility of interference between different ionization mechanisms was consistently included in the calculation. In a joint theory-and-experiment effort, the *R*-matrix method was recently applied with great success to the electron-impact single ionization of the Li-like C^{3+} [7] and O^{5+} [8] ions. In the present study we extend our work to Ne^{7+} ions, aiming at an assessment of the ion charge dependence of indirect ionization mechanisms along the Li-like sequence.

For electron-impact single ionization of Li-like Ne^{7+}, besides the direct ionization (DI)

$$e^- + \mathrm{Ne}^{7+}(1s^2 2s) \rightarrow \begin{cases} \mathrm{Ne}^{8+}(1s^2) + 2e^- \\ \mathrm{Ne}^{8+}(1s2s) + 2e^-, \end{cases} \quad (1)$$

three indirect mechanisms have to be considered: nonresonant excitation-autoionization (EA),

$$e^- + \mathrm{Ne}^{7+}(1s^2 2s) \rightarrow \mathrm{Ne}^{7+*}(1s2snl) + e^- \\ \hookrightarrow \mathrm{Ne}^{8+}(1s^2) + e^-, \quad (2)$$

resonant-excitation-double-autoionization (REDA),

$$e^- + \mathrm{Ne}^{7+}(1s^2 2s) \rightarrow \mathrm{Ne}^{6+*}(1s2snln'l') \\ \hookrightarrow \mathrm{Ne}^{7+*}(1s2sn''l'') + e^- \\ \hookrightarrow \mathrm{Ne}^{8+}(1s^2) + e^-, \quad (3)$$

and resonant-excitation-auto-double-ionization (READI),

$$e^- + \mathrm{Ne}^{7+}(1s^2 2s) \rightarrow \mathrm{Ne}^{6+*}(1s2snln'l') \\ \hookrightarrow \mathrm{Ne}^{8+}(1s^2) + 2e^-. \quad (4)$$

We note that the latter mechanism proceeds via simultaneous emission of two electrons. Figure 1 shows samples of different ionization pathways for the single ionization of the Ne^{7+} ion within an energy diagram.

Ionization of Ne^{7+} received attention previously. Experimentally, single ionization of Ne^{7+} was investigated by Donets and Ovzyannikov [9] by modeling charge-state evolution in an electron beam ion source, and in Refs. [10,11] using the crossed-beam technique. In addition to the direct ionization, only a gross indirect feature (EA) could be observed in the ionization cross section so far. The situation on the theoretical side is similar. Cross sections including contributions of DI and EA were calculated using the Coulomb-Born approximation by Jakubowicz and Moores [12] and the distorted wave Born exchange approximation by Chen *et al.* [13]. No calculation for the resonant indirect processes (REDA and READI) was available prior to the present work.

Here we report detailed experimental and theoretical re-

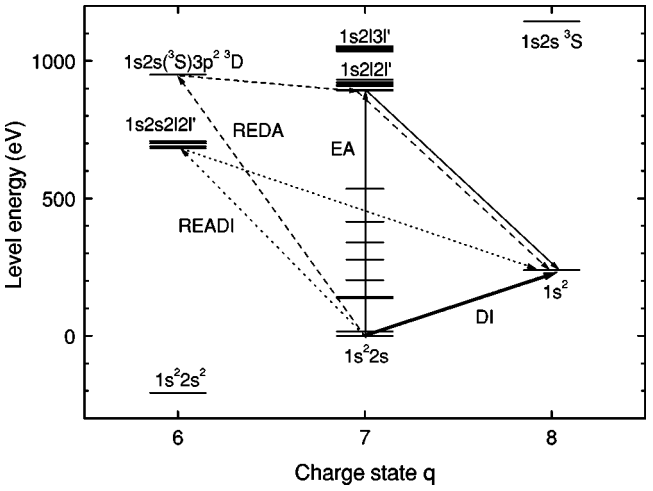

FIG. 1. Energy-level diagram of Ne^{q+} states relevant to the single ionization of Ne^{7+}. Horizontal bars indicate the energy levels (including five pseudostates represented by shorter bars) used in the present *R*-matrix calculation. Ionization pathways are indicated by different arrow lines. The fat solid arrow line shows the direct ionization (DI) channel; the thin solid arrow lines represent the excitation-autoionization (EA) channel; the dotted arrow lines indicate the resonant-excitation-auto-double-ionization (READI) channel; and the dashed arrow lines represent the resonant-excitation-double-autoionization (REDA) channel.

sults for the single ionization of Ne^{7+}. Our studies were devoted mainly to the resonant processes (READI and REDA) near the *K*-shell excitation (EA) threshold region. Autoionizing resonances were measured with a high precision and high energy resolution. The ionization cross sections were calculated using the unified *R*-matrix method [6–8], which treats processes (1)–(4) in a consistent manner.

The measurements were performed using the crossed-beams setup described previously in detail by Tinschert *et al.* [14]. Ne^{7+} ions were produced by a 10-GHz electron cyclotron resonance ion source [15]. A collimated (2×2 mm^2) 70-keV Ne^{7+} ion beam with a current up to 70 nA was crossed with an intense ribbon-shaped electron beam with currents as high as 450 mA at 1000 eV. After the interaction, the ionized product ions (Ne^{8+}) were separated from the incident beam by a magnetic field, and detected by a single-particle detector, while the parent ion beam was collected by a Faraday cup. The counting rate of the ionized Ne^{8+} ions was at the level of a few kHz.

For the observation of fine details in the ionization cross section, the electron-energy-scan technique [3,8] was employed. With an optimized overlap of the intersecting beams, the electron energy was ramped over preset ranges of typically 40 eV in 512 steps of 0.078 eV each, and a dwell time of 3 ms on each energy. The scans were automatically repeated until the counting statistics reached a desired level. Numerous individual overlapping energy scans were then combined, and the final relative scan measurement was obtained. Limited by the maximum cathode voltage that can be applied to the electron gun, the electron energy was below 1000 eV. In the present measurements, energy scans were made in two separate regions. The 660–720-eV scan covers the dominant READI resonances, and the 870–1000-eV region includes the most important REDA resonances as well as EA at the *K*-shell excitation threshold. The total number of counts per channel was roughly 1.5×10^6 and 1.5×10^5 for the lower- and higher-energy scan ranges, respectively. By combining packets of five neighboring original data points, effectively going to 0.39-eV stepwidth, statistical uncertainties were reduced to 0.036% and 0.12% for the lower- and higher-energy regions, respectively. READI resonances via intermediate states of the configuration $1s2s2l2l'$ and REDA resonances via intermediate states of the configuration $1s2s3lnl'$ were clearly observed. The present scan data were normalized to the absolute measurement of Duponchelle *et al.* [11], such that the cross sections from both experiments agree in the energy region below 890 eV where DI dominates. The error of the experimental energy scale is within 1.5 eV [16]. The role of electron-beam space charge in the determination of the energy was recently discussed in detail [8].

The unified *R*-matrix approach of Berrington *et al.* [6] has been adopted in the present work using an extended basis set for improved representation of the total wave function. Our approach was described in detail previously [7,8]. Briefly, a unified total wave function, which can represent the initial and final states required for the treatment of DI, EA, REDA, and READI processes, is constructed with a set of common orbitals. The real target states and the pseudostates are defined on the basis of these orbitals. For the Ne^{7+} ion, a total of 26 spectroscopic states and pseudostates were used. These include five physical bound states $1s^22s\,^2S$, $1s^22p\,^2P$, $1s^23s\,^2S$, $1s^23p\,^2P$, and $1s^23d\,^2D$, five pseudostates of the type $1s^2\overline{4s}\,^2S$, $1s^2\overline{4p}\,^2P$, $1s^2\overline{4d}\,^2D$, $1s^2\overline{4f}\,^2F$, and $1s^2\overline{5p}\,^2P$, as well as 16 $1s2l2l'$ and $1s2s3l'$ autoionizing states. All target states and pseudostates were represented by configuration-interaction (CI) wave functions. Eleven orbitals were used: the $1s$, $2s$, $2p$, $3s$, $3p$, and $3d$ orbitals were taken from the table given by Weiss [17], these orbitals also give good excited state wave functions; the $\overline{4s}$, $\overline{4p}$, $\overline{4d}$, and $\overline{4f}$ orbitals were optimized on the $1s2s^2$, $1s2p^2$, and $1s2s2p$ inner-shell excited states, using the CIV3 package of Hibbert [18]; and the $\overline{5p}$-polarized orbital was optimized on the $1s^22s$ ground-state dipole polarizability. The target orbitals require an *R*-matrix radius of 6.0 a.u., and 24 continuum basis functions were used per angular momentum. The internal region *R*-matrix package RMATRX II [19] and the external asymptotic program STGF [20] were employed. Partial waves up to total angular momentum $L=20$ were needed to obtain converged results for the ionization cross sections. A top-up procedure was used to check for possible contributions of higher partial waves, and they were found negligible. Finally, the total cross section for ionization from the ground state was calculated by summing the excitation cross sections for transitions into all the autoionizing states and pseudostates lying above the ionization threshold of the ground state, i.e., 239.10 eV [21].

As we pointed out in a recent paper [8], the present unified *R*-matrix method is unable to account for two loss mechanisms explicitly due to limitations in its basis set. The first is the radiative damping effect, and the second is the effect of flux loss into infinite Rydberg series of nonautoionizing states. It has been shown that radiative damping can reduce the contribution of the EA process significantly, but this effect is small for REDA and READI processes. In the present calculation the effect of radiation damping on the EA process has been corrected for by explicitly determining the branching ratios of the autoionizing states included in the calculation, using the same wave functions. The second loss mechanism results in a reduction of ionization strength of REDA and READI resonances just around and below the lowest EA threshold. Following the discussion in our recent work [8], resonances calculated for Ne^{7+} in the energy range 840–920 eV are therefore completely removed from the original calculation with the argument that the $1s2s2ln'l'$ intermediate states with $n'\geqslant 4$ most likely decay to singly excited (bound) $1s^2nl$ states of the Li-like system.

An overview of the experimental and theoretical cross sections for the single ionization of Ne^{7+} is given in Fig. 2. For the comparison with the experiment the results of the present calculation were convoluted with a Gaussian of a full width at half maximum of 3 eV. As can be seen from the figure, the DI part of the experimental results of Duponchelle *et al.* [11] is well reproduced by the Lotz formula [22]. The DI part of the calculation of Chen *et al.* [13] agrees very well with that of Jakubowicz and Moores [12], but both are about 15% lower than the experimental data of Duponchelle *et al.*

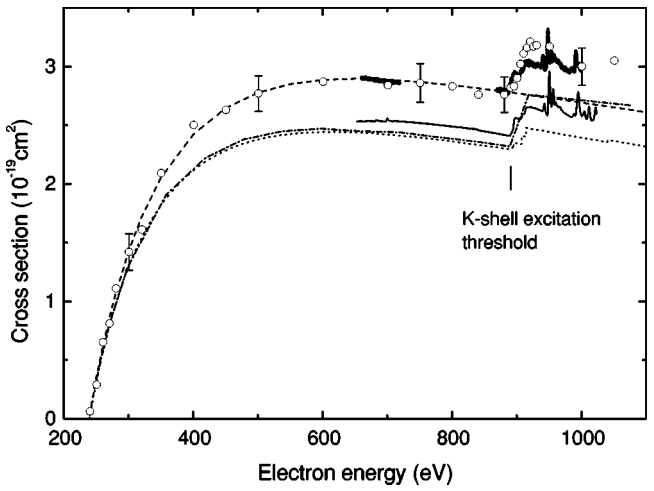

FIG. 2. Total electron-impact single-ionization cross sections of Ne^{7+}. Present experimental data (nonresolved solid dots), data of Duponchelle *et al.* [11] (open circles) with few representative experimental uncertainties indicated (sum of the statistical and systematic uncertainties). Shown are the present calculation (solid line), the calculation of Chen *et al.* [13] (dotted line), the calculation of Jakubowicz and Moores [12] (dash-dotted line), and the Lotz formula [22] (dashed line).

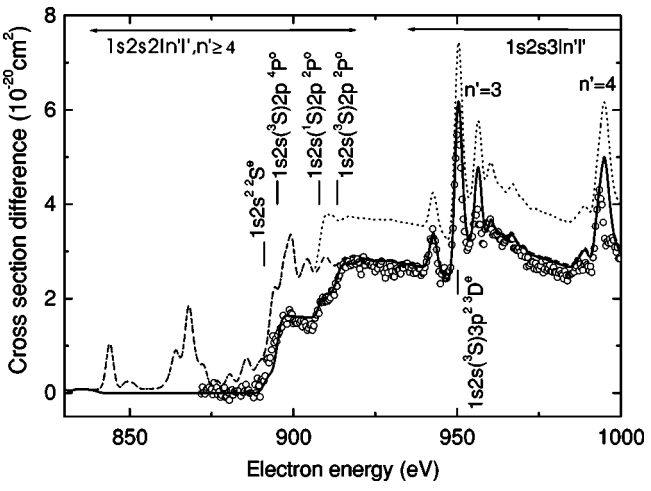

FIG. 3. Indirect contribution ($\Delta\sigma$) to the cross section for electron-impact single ionization of Ne^{7+}(830–1000 eV). Open circles represent the present experiment (the statistical errors are about 9×10^{-22} cm^2); the present calculation before any correction for loss mechanisms is shown by the dotted line; the present calculation after correction for radiation damping only is shown by the dashed line; and the final result of the present calculation is shown by the solid line. Theoretical positions of the most important EA thresholds and dominant REDA resonances are indicated by vertical bars. The arrow line shows the energy region of possible REDA resonances associated with $1s2s3ln'l'$ intermediate states, and that of possible READI resonances associated with $1s2s2ln'l'$ intermediate states for $n'\geqslant4$.

The present theoretical result for DI is between the results of the other two calculations and the experimental data. Concerning the EA contribution (the step feature at 891 eV), our calculation agrees well with our scan measurement (see below for detailed comparison), and it is between the calculation of Chen *et al.* and that of Jakubowicz and Moores.

In the following figures, indirect contributions rather than total cross sections σ^{exp} are displayed. In order to extract the indirect contribution (the cross-section difference $\Delta\sigma=\sigma^{expt}-\sigma_{DI}$), the DI contribution σ_{DI} is subtracted from the total cross sections. This procedure involves uncertainty of the overall size of $\Delta\sigma$, since σ_{DI} is not measured separately. However, for the present purpose of studying resonant ionization processes, this allows for the most sensitive comparison of details in the present theory and experiment. For the theoretical data, the DI cross sections were calculated using the nonunified *R*-matrix method. Concerning the experimental data, the DI contribution is not measured separately, but can be obtained indirectly. It is apparent from Fig. 2 that the Lotz calculation of σ_{DI} [22] happens to be in very good agreement with the DI part of the experimental data, and was therefore used to determine $\Delta\sigma$ for the higher-energy region. As for the lower-energy region (660–720 eV), the smooth part of the cross section was fitted with a straight line, which was used as the DI contribution to be subtracted.

Figure 3 shows the indirect ionization contribution in the energy region 830–1000 eV. Given in the figure are results of the present measurement and calculation. Calculations with and without corrections for the loss mechanisms are displayed. Very good agreement between the measurement and the final theoretical result is found both in the size and shape of the cross section details. As for the positions of the resonances, calculations and measurements differ by less than 1.5 eV. Resonances in the cross sections of the present energy region belong to REDA processes via intermediate excited states $1s2s3ln'l'$, with $n'=3$ and 4. Fine structures within the $1s2s3l3l'$ manifold are resolved with the dominant resonance identified as $1s2s(^3S)3p^2\,^3D^e$ at 950.20 eV, with a substantial admixture of $1s2s(^3S)3s3d\,^3D^e$ due to configuration interaction. The contribution of this resonance

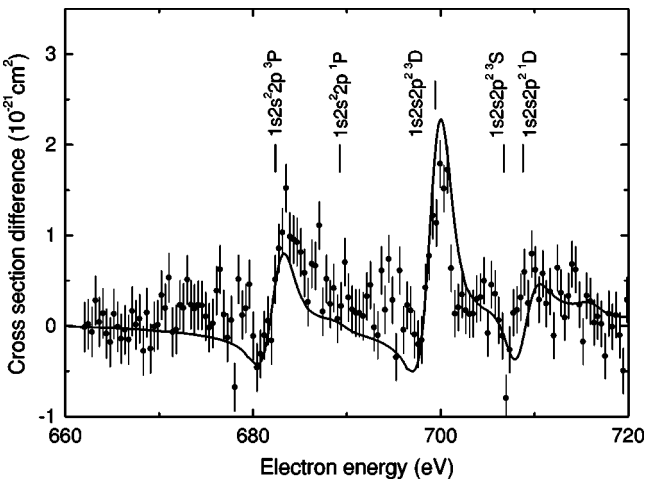

FIG. 4. Indirect contribution ($\Delta\sigma$) to the cross section for electron-impact single ionization of Ne^{7+}(660–720 eV). Solid dots represent the present experiment (error bars are statistical only); the solid line shows the present theory. Theoretical positions of the dominant READI resonances are indicated by vertical bars.

at the peak energy reaches 10% of the total cross section. In addition to the REDA processes, four EA steps associated with $1s2s2l$ resonant excitations are visible. They were identified to be due to multiply excited states $1s2s^2\,^2S^e$ at 891.05 eV, $1s2s(^3S)2p\,^4P^o$ at 895.05 eV, $1s2s(^1S)2p\,^2P^o$ at 907.85 eV, and $1s2s(^3S)2p\,^2\mathrm{P}^o$ at 913.33 eV. Within the systematic experimental uncertainties these calculated threshold energies agree with the energies of the EA steps in the experimental data. The nonresonant indirect contribution amounts to about 10% of the total ionization cross section. Thus the total indirect contribution observed in the experiment at the top of the $1s2s(^3S)3p^2\,^3D^e$ at 950 eV is more than 20% of the total single-ionization cross section.

Figure 4 takes a closer look at the lower-energy region. In the energy region below the $1s2s^2$ EA threshold, REDA is energetically not possible, and only READI processes via the $1s2s2ln'l'$ intermediate states are allowed. Theory predicts five READI resonances via intermediate states $1s2s^22p\,^3P^o$, $1s2s^22p\,^1P^o$, $1s2s2p^2\,^3D^e$, $1s2s2p^2\,^3S^e$, and $1s2s2p^2\,^1D^e$ at energies of 682.39, 689.24, 699.43, 706.74, and 708.77 eV, respectively. In the experimental data only two main resonance features are visible. They are well reproduced by the theory. Similar to the observations with C^{3+} [7] and O^{5+} [8], the second main READI resonance belonging to $1s2s2p^2\,^3D$ is again overestimated by the theory. The three weaker resonances predicted by the theory are not immediately obvious in the experimental data because of the limited counting statistics. At the peak of the experimental data, the READI process contributes 0.5% of the total ionization cross section. The theoretical result clearly shows interference between the DI and READI channels. The experimental data in general support this prediction, but even better counting statistics would be needed for a more solid conclusion.

In summary, indirect ionization processes including READI and REDA resonances have been investigated in great detail both experimentally and theoretically for the Ne^{7+} ion. REDA resonances via intermediate excited states $1s2s3ln'l'$ with $n'=3$ and 4 and READI resonances via intermediate excited states $1s2s2l2l'$ have been observed. The present *R*-matrix approach including some *ad hoc* corrections reproduces the experimental results remarkably well.

We thank Professor P. G. Burke for providing us with a copy of the RMATRX II package, and Dr. S. Schippers for helpful discussions. Support by Deutsche Forschungsgemeinschaft, Bonn, is gratefully acknowledged.

[1] K. J. LaGattuta and Y. Hahn, Phys. Rev. A **24**, 2273 (1981).
[2] R. J. W. Henry and A. Z. Msezane, Phys. Rev. A **26**, 2545 (1982).
[3] A. Müller *et al.*, Phys. Rev. Lett. **61**, 70 (1988).
[4] A. Müller *et al.*, Phys. Rev. Lett. **61**, 1352 (1988).
[5] D. L. Moores and K. J. Reed, Adv. At., Mol., Opt. Phys. **34**, 301 (1994).
[6] K. A. Berrington, J. Pelan, and L. Quigley, J. Phys. B **30**, 4973 (1997).
[7] H. Teng *et al.*, Phys. Rev. A **61**, 060704(R) (2000).
[8] A. Müller, H. Teng, H. Hofmann, R. A. Phaneuf, and E. Salzborn, Phys. Rev. A **62**, 062720 (2000).
[9] E. D. Donets and V. P. Ovzyannikov, Zh. Éksp. Teor. Fiz. **80**, 916 (1981) [Sov. Phys. JETP **53**, 466 (1981)].
[10] P. Defrance, S. Chantrenne, S. Rachafi, D. S. Belií, J. Jureta, D. C. Gregory, and F. Brouillard, J. Phys. B **23**, 2333 (1990).
[11] M. Duponchelle, M. Khouilid, E. M. Oualim, H. Zhang, and P. Defrance, J. Phys. B **30**, 729 (1997).
[12] H. Jakubowicz and D. L. Moores, J. Phys. B **14**, 3733 (1981).
[13] C. Y. Chen *et al.*, J. Phys. B **31**, 2667 (1998).
[14] K. Tinschert, A. Müller, G. Hofmann, K. Huber, R. Becker, D. C. Gregory, and R. Salzborn, J. Phys. B **22**, 531 (1989).
[15] M. Liehr, M. Schlapp, R. Trassel, G. Hofmann, M. Stenke, R. Völpel, and E. Salzborn, Nucl. Instrum. Methods Phys. Res. B **79**, 697 (1993).
[16] G. Hofmann, A. Müller, K Tinschert, and E. Salzborn, Z. Phys. D: At., Mol. Clusters **16**, 113 (1990).
[17] A. W. Weiss, Astrophys. J. **138**, 1262 (1963).
[18] A. Hibbert, Comput. Phys. Commun. **9**, 141 (1975).
[19] P. G. Burke, V. M. Burke, and K. M. Dunseath, J. Phys. B **27**, 5341 (1994).
[20] M. J. Seaton, J. Phys. B **18**, 2111 (1985).
[21] NIST Atomic Spectra Database web site: http://physics.nist.gov/cgi−bin/AtData/levels_form
[22] W. Lotz, Z. Phys. **232**, 101 (1970).